Detailed seismic imaging of Merapi volcano, Indonesia, from local earthquake travel-time tomography

Mohamad Ramdhan[a,b], Sri Widiyantoro[c,d*], Andri D. Nugraha[c], Jean-Philippe Métaxian[e,f], Nicholas Rawlinson[g], Asep Saepuloh[h], Said Kristyawan[a,b], Andry S. Sembiring[a,b], Agus Budi-Santoso[i], Antoine Laurin[e], Ahmad A. Fahmi[e]

[a] *Study Program of Earth Science, Faculty of Earth Sciences and Technology, Institut Teknologi Bandung, Jalan Ganesa No. 10, Bandung 40132, Indonesia*

[b] *Agency for Meteorology, Climatology and Geophysics, Jalan Angkasa I, No. 2, Kemayoran, Jakarta, Indonesia*

[c] *Global Geophysics Research Group, Faculty of Mining and Petroleum Engineering, Institut Teknologi Bandung, Jalan Ganesa No. 10, Bandung 40132, Indonesia*

[d] *Research Center for Disaster Mitigation, Institut Teknologi Bandung, Jalan Ganesa No. 10, Bandung 40132, Indonesia*

[e] *ISTerre, IRD R219, CNRS, Université de Savoie Mont Blanc, Le Bourget-du-Lac, France*

[f] *Institut de Physique du Globe de Paris, Université Sorbonne-Paris-Cité, CNRS, France*

[g] *Department of Earth Sciences – Bullard Labs, University of Cambridge, Cambridge CB30EZ, United Kingdom*

[h] *Faculty of Earth Sciences and Technology, Institut Teknologi Bandung, Jalan Ganesa No. 10, Bandung 40132, Indonesia*

[i] *Center for Volcanology and Geological Hazard Mitigation, Geological Agency, Jalan Diponegoro No. 57, Bandung, 40122, Indonesia*

**Corresponding author: sriwid@geoph.itb.ac.id*

A B S T R A C T

Mt. Merapi, located in central Java, Indonesia, is one of the most active volcanoes in the world. It has been subjected to numerous studies using a variety of methods, including tomographic imaging, in an attempt to understand the structure and dynamics of its magmatic plumbing system. Results of previous seismic tomographic studies that include Mt. Merapi poorly constrain the location of its underlying magma source due to limited data coverage. In order to comprehensively understand the internal structure and magmatism of Mt. Merapi, a project called DOMERAPI was conducted, in which 53 broadband seismic stations were deployed around Mt. Merapi and its neighbourhood for approximately 18 months, from October 2013 to April 2015. In this study, we compare Vp, Vs, and Vp/Vs tomograms constructed using data obtained from local (DOMERAPI) and regional seismic networks with those obtained without DOMERAPI data. We demonstrate that the data from the DOMERAPI seismic network are crucial for resolving key features beneath the volcano, such as high Vp/Vs ratios beneath the Merapi summit at ~5 km and ~15 km depths, which we interpret as shallow and intermediate magma bodies, respectively. Furthermore, west-east vertical sections across Mt. Merapi, and a “dormant” (less active)

volcano, Mt. Merbabu, exhibit high Vp/Vs and low Vp/Vs ratios, respectively, directly beneath their summits. This observation likely reflects the presence (for Mt. Merapi) and absence (for Mt. Merbabu) of shallow magma bodies near the surface.

Keywords:

DOMERAPI

Merapi

Merbabu

Tomography

1. Introduction

The origin of Mt. Merapi, located in the central part of Java in the eastern Sunda arc of Indonesia, can be traced back to the subduction of the Indo-Australian plate beneath the Eurasian plate (Widiyantoro et al., 2011; Widiyantoro and van der Hilst, 1996). This volcano is one of the most active stratovolcanoes in the world, with an eruption frequency of between two to six years. For example, eruptions occurred in 1984, 1986, 1992, and 1994 (Ratdomopurbo and Poupinet, 2000). Very large eruptions tend to occur with a frequency of between 50 to 100 years (Lühr et al., 2013; Surono et al., 2012). Eruptions of the Merapi volcano are usually dominated by pyroclastic flows caused by the collapse of the lava dome (Hidayati et al., 2008). However, a large

eruption in 2010 exhibited a number of features that had not previously been observed in past eruptions. For instance, the initial eruption was explosive with a rating of ~4 (Komorowski et al., 2013; Surono et al., 2012) on the Volcanic Explosivity Index (VEI), reflecting the sizable volume of ejecta that was liberated. The frequency and size of eruptions that characterize Mt Merapi has attracted a range of researchers from different disciplines to study the ongoing activity at and below the summit of this unique volcano.

The results of the 2004 MERapi AMphibious EXperiment (MERAMEX) project were successful in explaining the relationship between the volcanic arc and the subduction zone in central Java. For instance, P- and S-wave velocity anomalies appear to depict the migration pathway of fluid or molten rocks from the partial melting zone at depth toward the surface beneath the volcanic arc (Haberland et al., 2014; Koulakov et al., 2007; Wagner et al., 2007). The results of these studies have been updated using additional data from the Indonesian Meteorological, Climatological and Geophysical Agency (BMKG) catalogue (Rohadi et al., 2013). However, even this more recent investigation has not been able to image the magma reservoirs beneath Merapi in any detail due to a lack of seismic data coverage. More localized studies using volcano-tectonic earthquake data show that volcanic events occur down to depths of ~5 km below the summit of Mt. Merapi (Budi-Santoso et al., 2013; Hidayati et al., 2008; Ratdomopurbo and Poupinet, 2000), which means that seismic velocity structure at depths >~5 km cannot be determined using these shallow events.

The DOMERAPI project, which involved the deployment of 53 broadband seismic stations around Mt. Merapi between 2013 and 2015, was carried out in

part to image magma bodies beneath the volcano in unprecedented detail. Widiyantoro et al. (2018) used relocated events from the DOMERAPI and BMKG networks (Ramdhan et al., 2017) to investigate the magma plumbing system beneath Merapi. In this study, we have carried out seismic tomography using the DOMERAPI data combined with data recorded by other seismic networks, including the BMKG network, the MERAMEX network and the Indonesian Institute for Research and Development of Geological Disaster Technology (BPPTKG) network. Our results clearly demonstrate that the inclusion of the DOMERAPI data significantly improves the imaging of possible magma bodies.

2. Data and methodology

2.1. Data

In this study, we have combined data from the DOMERAPI, BMKG, MERAMEX, and BPPTKG seismic networks to maximize the data coverage around the Merapi area. We used the BMKG and BPPTKG data from the same recording period as the DOMERAPI project period, i.e. from October 2013 to April 2015. In the case of MERAMEX, data were collected from May to September 2004. Fig. 1 shows the distribution of the four seismic networks used in this study.

In total, 942 events were extracted from the four seismic networks; 464 earthquakes were recorded by the DOMERAPI and BMKG seismographic stations in the same period, 260 of which were also recorded by the BPPTKG stations. The total number of earthquakes recorded by the MERAMEX stations

was 282. The remaining 196 events were taken from the BMKG catalog beyond the DOMERAPI recording period in order to minimize the azimuthal gap in the hypocenter determination process. All earthquakes were relocated prior to tomographic inversion. The total number of earthquakes that were successfully relocated is 794, with the remaining 148 discarded due to poor data fit. A detailed analysis of event locations from the DOMERAPI and BMKG networks is available in Ramdhan et al. (2017).

The earthquake data used for tomography are restricted to the longitude and latitude ranges 108^0-112^0E and 6^0-11^0S, respectively (Fig. 2). For this region, we end up with a total of 767 relocated events that were recorded by 254 seismographic stations (53 from DOMERAPI, 17 BMKG, 167 MERAMEX, and 17 BPPTKG seismometers). Each earthquake used for tomographic inversion is recorded by at least six seismographic stations. Fig. 2 shows the distribution of epicenters, seismometers, and the inversion grid (which is used to define variations in velocity structure) employed in this study (see Figs. S1 and S2 in the Supplementary Materials for the distribution of hypocenters and ray paths).

2.2. Methodology

For this study, hypocenters were located using the Geiger method (Geiger, 1912), as implemented in the Hypoellipse program (Lahr, 1999). This technique was successfully applied to map earthquake distribution along several faults in western Java by Supendi et al. (2018). For a reference velocity model (see Table 1), we adopted the 1-D P-wave velocity model of Koulakov et al. (2007) and used a Vp/Vs ratio of 1.73 taken from Ramdhan et al. (2017). The hypocenter

relocation technique employed in this study is the double-difference method (Waldhauser, 2001; Waldhauser and Ellsworth, 2000). Previously, this method was also successfully applied to relocate earthquakes from the BMKG catalog in several other regions in Indonesia (Cahyaningrum et al., 2015; Ramdhan and Nugraha, 2013; Sabtaji and Nugraha, 2015; Utama et al., 2015). To conduct the travel-time tomography, we used the SIMULPS12 codes (Eberhart-Phillips, 1993; Evans et al., 1994), which have been widely used to image subsurface structure in many parts of the world. For instance, they were used in the study of Nugraha and Mori, 2006, who clearly detected the subducted slab beneath the Shikoku and Bungo channels in Japan. Furthermore, these codes were also used by Nugraha et al., 2015, who managed to clearly detect a subducting slab beneath the Bali, Lombok, and Sumbawa Islands in the eastern Sunda arc. SIMULPS12 was also successfully applied to delineate structure beneath several Indonesian volcanoes, including Mt. Lokon in Sulawesi by Firmansyah et al. (2015) and Mt. Guntur in western Java by Nugraha et al. (2013). Inversions were performed for Vp and Vp/Vs ratio simultaneously. Determination of Vp/Vs ratio via direct inversion of S-P arrival time differences is more reliable compared to separately inverting for Vs and then dividing Vp by Vs, because in general the quality of S data is not as good as the quality of P data (Eberhart-Phillips, 1993). Moreover, Vp and Vp/Vs tomograms are very useful for interpreting not only structural features, but also the physical properties of rocks. The computation of the 3-D seismic velocity structure beneath Mt. Merapi and its surrounding areas used a relatively small grid spacing of 10 km in the horizontal direction and 5 km in the vertical direction down to 35 km depth. For greater depths, where the data coverage is more sparse,

we used a coarser grid spacing (Table 2). For selecting optimal damping values we constructed trade-off curves showing model variance versus data variance, as displayed in Fig. 3.

3. Tomographic imaging results

In this section, we present our final Vp, Vs, and Vp/Vs tomograms along with resolution test results. We also demonstrate that the inclusion of the DOMERAPI data set produces significant improvements in the recovery of detailed structure beneath Mt. Merapi.

3.1. Resolution tests

Resolution tests were conducted to understand which structural features can be resolved by the data. In this study, we employed conventional checkerboard tests. Positive and negative perturbations of ± 10% relative to the 1-D reference velocity model were used as inputs in the tests. If the inversion results show that one grid/block has the same anomaly (positive or negative) as the input model, even with a reduction in amplitude due to the implementation of damping, we consider that block to be resolved by the data. We can then interpret those parts of the model that are considered to be resolved by this approach, while keeping in mind the limitations of the checkerboard test in assessing the resolution of tomograms (Lévěque et al., 1993, Rawlinson and Spakman, 2016). Here, we emphasize the improved resolution due to the incorporation of the DOMERAPI data.

3.2. Vp, Vs, and Vp/Vs tomograms

To recover the seismic velocity structure beneath the Merapi volcano and its surroundings, we used a total of 29,937 (20,185 P and 9,752 S) ray paths from local events. Vp anomalies are stated in percent (perturbations) relative to the 1-D initial velocity model used in the inversion, whereas Vp/Vs ratios are in absolute values. The Vp/Vs ratio is directly proportional to Poisson's ratio, which is sensitive to temperature and the presence of fluid. The presence of magma or molten material is typically characterised by a high Vp/Vs ratio (see e.g. Nakajima et al., 2001). Regions of the model that will be discussed are only those with good resolution based on the checkerboard test results.

The pattern of anomalies that characterise the Vp and Vp/Vs models may well be different because the Vp/Vs model strongly depends on Vs, which is a more sensitive indicator of fluids compared to Vp. Therefore, we present not only Vp and Vp/Vs models, but also the Vs model. In the following, west-east vertical sections across Mt. Merbabu and Mt. Merapi are presented in order to directly compare the internal structures of these two volcanoes. In Fig. 4 (a-c), we display A-A' vertical sections through Vp, Vs, and Vp/Vs models from joint inversions using the DOMERAPI, MERAMEX, BMKG, and BPPTKG data. We also show similar cross sections, but derived by excluding the DOMERAPI data (Fig. 4 d-f). The differences between these sections are plotted with a more restricted perturbation scale to highlight the improvement due to the inclusion of DOMERAPI data (Fig. 4 g-i). The results of checkerboard tests for the associated cross sections are presented in Fig. 5. Here, we also demonstrate the improved checkerboard recovery owing to the inclusion of the DOMERAPI data, which are

quite pronounced for the region beneath Merapi. A similar presentation of tomograms is given in Fig. 6 for west-east (B-B') vertical sections across Merapi from the Vp, Vs, and Vp/Vs models. The corresponding checkerboard resolution test results are displayed in Fig. 7. Map views are also presented in Figs. 8 and 9, i.e. horizontal slices at 5 km depth through the Vp, Vs, and Vp/Vs models along with the corresponding checkerboard resolution test results. Horizontal slices across a range of depths are also presented in Figs. S3 and S4. The results of resolution tests in which Gaussian noise is added to the synthetic data are shown in Figs. S5 and S6. In what follows, we discuss and interpret these tomograms, with a focus on the possible existence of magma bodies beneath the Merapi volcano.

4. Discussion

In this section, we concentrate our discussion on the internal structures of Mt. Merbabu and Mt. Merapi, which represent "dormant" and active volcanoes, respectively. We also discuss the significant improvement in the resulting tomographic images owing to the incorporation of the DOMERAPI data.

4.1. Mt. Merbabu vs Mt. Merapi

The west-east (A-A') vertical sections through Vp, Vs, and Vp/Vs models shown in Fig. 4 depict the internal structure of Mt. Merbabu. A low Vp/Vs ratio is observed from the summit to depths of ~20 to ~25 km below mean sea level (MSL), a region which the checkerboard test results suggest is well resolved (Fig. 5). The low Vp/Vs ratio directly beneath the summit down to a depth of ~5 km is

associated with high Vp and higher Vs. On the other hand, the low Vp/Vs ratio at greater depths is due to very low Vp and low Vs (cf. Widiyantoro et al., 2018). These anomalies are unlikely to be related to the presence of fluids or melts, which is consistent with the fact that Mt. Merbabu is not currently active, with the last known activity being a moderate eruption that occurred in 1797 (van Hinloopen Labberton, 1921). This last eruption was rated 2 on the VEI (cf. VEI ~4 for the Merapi eruption of 2010 ; Komorowski et al., 2013; Surono et al., 2012).

Fig. 6 also displays west-east vertical sections through the Vp, Vs, and Vp/Vs models, but across Mt. Merapi (B-B'). In contrast to Fig. 4, we evidently have a high Vp/Vs ratio beneath the summit down to a depth of ~5 km below MSL, which is due to low Vp and very low Vs. In addition, we also observe a very high Vp/Vs ratio at a depth of ~15 km that is associated with high Vp and low Vs anomalies. The results of the checkerboard tests displayed in Fig. 7 indicate that in general, structures beneath Merapi are well resolved down to a depth of ~25 km, particularly when the DOMERAPI data are included. We interpret the high Vp/Vs ratio as being related to the presence of fluids or melts, while the deeper high Vp/Vs ratio is interpreted as an intermediate magma reservoir, as suggested by Costa et al., 2013 based on petrological studies.

The internal structures of Mt. Merbabu and Mt. Merapi are much more clearly imaged when the DOMERAPI data are included, as illustrated by the difference between models derived with and without this data set. The most intriguing features are the shallow and intermediate high Vp/Vs ratios beneath Merapi that are constrained by the DOMERAPI data (Fig. 6 i). These structural

features are well resolved (see Fig. 7 f). We interpret these two anomalies as shallow and intermediate magma bodies that underlie Merapi. Costa et al. (2013) also suggest the existence of an even deeper reservoir, at approximately the depth of the Moho. However, the presence or absence of such a deep reservoir cannot be determined by the data set used in this study, which do not constrain the lowermost crust or uppermost mantle

The 5 km depth slices through the Vp, Vs, and Vp/Vs tomograms depict two distinct features: (i) low Vp and Vs anomalies in the neighbourhood of the Merapi and Merbabu complex, and (ii) a high Vp/Vs ratio below Merapi, but not beneath Merbabu. The first observation, in particular the strong low velocity zone east of Merapi and Merbabu, is in good agreement with the important finding by Koulakov et al., 2007 of a very low Vp and Vs anomaly beneath central Java, called the Merapi-Lawu Anomaly. The second observation of the high and low Vp/Vs ratios beneath Merapi and Merbabu, respectively, is likely related to Merapi being an active volcano and Merbabu being “dormant”.

4.2. Improved resolution due to the inclusion of DOMERAPI data

In Figs. 4-9, we demonstrate the important contribution of the DOMERAPI seismic network in improving the resolution of Vp and Vp/Vs models, especially underneath Mt. Merapi. Compared with a number of previous studies which used travel-time tomography (e.g. Wagner et al. 2007; Koulakov et al. 2007; Rohadi et al. 2013; Haberland et al. 2014), the inclusion of the DOMERAPI data illuminates the magma system below the Merapi volcano in much more detail. From the checkerboard test results, it is clearly seen that the seismic resolution beneath

Merapi and its surroundings is greatly enhanced, especially in the crust (< 25 km); see Figs. 5 and 7. For the sake of completeness, we also include slices from deeper regions of the models and their associated resolution tests in Figs. S7 and S8.

5. Concluding Remarks

The additional data set from the DOMERAPI seismic network has significantly increased seismic ray coverage and hence the resolution of structural features beneath the Merapi volcano, especially for depths above 25 km. The incorporation of this new data set has permitted us to observe several important structural features in unprecedented detail, therefore allowing us to produce a more reliable interpretation. In particular, we detected the presence of shallow and intermediate magma bodies as indicated by high Vp/Vs ratios beneath Mt. Merapi. In contrast to Mt. Merapi, however, the internal structure of Mt. Merbabu is dominated by high velocity anomalies and a low Vp/Vs ratio, confirming that Merbabu is much less active than Merapi.

In future studies, we will conduct Qp and Qs tomographic investigations using the same data set; this will complement our current results because Q is more sensitive to temperature and the presence of fluids compared to seismic velocities. Moreover, seismic velocity and attenuation (1/Q) anomalies can be more reliably interpreted in terms of temperature variations by making use of constraints from laboratory studies of rock properties at different temperatures and pressures.

Acknowledgements

We are grateful to the French National Research Agency and Institut de recherche pour le développemen for funding the DOMERAPI project. We would also like to express our gratitude to PVMBG as the main partner of the DOMERAPI project in Indonesia, and BMKG for providing us with the earthquake data catalog used in this study. Thanks go to GFZ for granting access to the MERAMEX data, and *Lembaga Pengelola Dana Pendidikan* (LPDP), the Republic of Indonesia, for granting a doctoral scholarship to MR. This study was also supported in part by Direktorat Perguruan Tinggi (DIKTI), the Republic of Indonesia, through a WCU research grant 2016/2017, and a 2018 research grant from Institut Teknologi Bandung (ITB) awarded to SW. We are grateful for the constructive and helpful comments from the two anonymous reviewers. All images in this paper were plotted using the GMT program (Wessel and Smith, 1998).

References

Budi-Santoso, A., Lesage, P., Dwiyono, S., Sumarti, S., Subandriyo, Surono, Jousset, P., Metaxian, J.-P., 2013. Analysis of the seismic activity associated with the 2010 eruption of Merapi Volcano, Java. J. Volcanol. Geotherm. Res. 261, 153–170. https://doi.org/10.1016/j.jvolgeores.2013.03.024.

Cahyaningrum, A.P., Nugraha, A.D., Nanang, T.P., 2015. Earthquake hypocenter relocation using double difference method in East Java and surrounding areas. AIP Conf. Proc. 1658, 030021. https://doi.org/10.1063/1.4915029.

Costa, F., Andreastuti, S., Bouvet de Maisonneuve, C., Pallister, J.S., 2013. Petrological insights into the storage conditions, and magmatic processes that yielded the centennial 2010 Merapi explosive eruption. J. Volcanol. Geotherm. Res. 261, 209–235. https://doi.org/10.1016/j.jvolgeores.2012.12.025.

Eberhart-Phillips, D., 1986. Three-dimensional velocity structure in northern California Coast Ranges from inversion of local earthquake arrival times. Bull. Seismol. Soc. Am. 76, 1025–1052.

Eberhart-Phillips, D., 1993. Local earthquake tomography: earthquake source regions. Seismic Tomography: Theory and Practice 613–643.

Evans, J.R., Eberhart-Phillips, D., Thurber, C., 1994. User's manual for SIMULPS12 for imaging Vp and Vp/Vs; a derivative of the " Thurber" tomographic inversion SIMUL3 for local earthquakes and explosions. U. S. Geol. Surv. Open File Rep. 94–431.

Firmansyah, R., Nugraha, A.D., Kristianto, 2015. The preliminary results: Internal seismic velocity structure imaging beneath Mount Lokon. AIP Conf. Proc. 1658, 050012. https://doi.org/10.1063/1.4915051.

Geiger, L., 1912. Probability method for the determination of earthquake epicenters from the arrival time only. Bull. St. Louis Univ. 8, 56–71.

Haberland, C., Bohm, M., Asch, G., 2014. Accretionary nature of the crust of Central and East Java (Indonesia) revealed by local earthquake travel-time tomography. J. Asian Earth Sci. 96, 287–295. https://doi.org/10.1016/j.jseaes.2014.09.019.

Hidayati, S., Ishihara, K., Iguchi, M.M., Ratdomopurbo, A., 2008. Focal mechanism of volcano-tectonic earthquakes at Merapi volcano, Indonesia. Indones. J. Phys.19(3), 75–82.

Komorowski, J.-C., Jenkins, S., Baxter, P.J., Picquout, A., Lavigne, F., Charbonnier, S., Gertisser, R., Preece, K., Cholik, N., Budi-Santoso, A., Surono, 2013. Paroxysmal dome explosion during the Merapi 2010 eruption: Processes and facies relationships of associated high-energy pyroclastic density currents. J. Volcanol. Geotherm. Res. 261, 260–294. https://doi.org/10.1016/j.jvolgeores.2013.01.007.

Koulakov, I., Bohm, M., Asch, G., Lühr, B.-G., Manzanares, A., Brotopuspito, K.S., Fauzi, P., Purbawinata, M.A., Puspito, N.T., Ratdomopurbo, A., Kopp, H., Rabbel, W., Shevkunova, E., 2007. P and S velocity structure of the crust and the upper mantle beneath central Java from local tomography inversion. J. Geophys. Res. 112, B08310. https://doi.org/10.1029/2006JB004712.

Lahr, J., 1999. Revised 2012, HYPOELLIPSE: A computer program for determining local earthquake hypocentral parameters, magnitude, and first-motion pattern. U. S. Geol. Surv. Open File Rep. 99-23. https://doi.org/10.3133/ofr9923.

Lévěque, J.-J., Rivera, L., Wittlinger, G., 1993. On the use of the checker-board test to assess the resolution of tomographic inversions. Geophys. J. Int. 115, 313–318. https://doi.org/10.1111/j.1365-246X.1993.tb05605.x.

Lühr, B.-G., Koulakov, I., Rabbel, W., Zschau, J., Ratdomopurbo, A., Brotopuspito, K.S., Fauzi, P., Sahara, D.P., 2013. Fluid ascent and magma

storage beneath Gunung Merapi revealed by multi-scale seismic imaging. J. Volcanol. Geotherm. Res. 261, 7–19. https://doi.org/10.1016/j.jvolgeores.2013.03.015

Nakajima, J., Matsuzawa, T., Hasegawa, A., Zhao, D., 2001. Three-dimensional structure of Vp, Vs, and Vp/Vs beneath northeastern Japan: Implications for arc magmatism and fluids. J. Geophys. Res. 106, 21843-21858. DOI: 10.1029/2000JB000008

Nugraha, A.D., Kusnandar, R., Puspito, N.T., Sakti, A.P., Yudistira, T., 2015. Preliminary results of local earthquake tomography around Bali, Lombok, and Sumbawa regions. AIP Conf. Proc. 1658, 030019. https://doi.org/10.1063/1.4915027.

Nugraha, A.D., Mori, J., 2006. Three-dimensional velocity structure in the Bungo Channel and Shikoku area, Japan, and its relationship to low-frequency earthquakes. Geophys. Res. Lett. 33, L24307. https://doi.org/10.1029/2006GL028479.

Nugraha, A.D., Widiyantoro, S., Gunawan, A., Suantika, G., 2013. Seismic Velocity Structures beneath the Guntur Volcano Complex, West Java, Derived from Simultaneous Tomographic Inversion and Hypocenter Relocation. J. Math. Fund. Sci. 45(1), 17–28.

Ramdhan, M., Nugraha, A.D., 2013. Study of seismicity around Toba area based on relocation hypocenter result from BMKG catalogue. AIP Conf. Proc. 1554, 242. https://doi.org/10.1063/1.4820330.

Ramdhan, M., Widiyantoro, S., Nugraha, A.D., Métaxian, J.-P., Saepuloh, A., Kristyawan, S., Sembiring, A.S., Santoso, A.B., Laurin, A., Fahmi, A.A.,

406 2017. Relocation of hypocenters from DOMERAPI and BMKG networks:
407 a preliminary result from DOMERAPI project. Earthq. Sci.
408 https://doi.org/10.1007/s11589-017-0178-3.
409Ratdomopurbo, A., Poupinet, G., 2000. An overview of the seismicity of Merapi
410 volcano (Java, Indonesia), 1983–1994. J. Volcanol. Geotherm. Res. 100,
411 193–214. https://doi.org/10.1016/S0377-0273(00)00137-2.
412Rawlinson, N., Spakman, W., 2016. On the use of sensitivity tests in seismic
413 tomography, Geophys. J. Int. 205(2), 1221–1243. DOI:
414 10.1093/gji/ggw084.
415Rohadi, S., Widiyantoro, S., Nugraha, A.D., Masturyono, 2013. Tomographic
416 imaging of P- and S-wave velocity structure beneath central Java,
417 Indonesia: Joint inversion of the MERAMEX and MCGA earthquake data.
418 Int. J. Tomogr. Stat. 24(3), 1–16.
419Sabtaji, A., Nugraha, A.D., 2015. 1-D seismic velocity model and hypocenter
420 relocation using double difference method around West Papua region. AIP
421 Conf. Proc. 1658, 030005. https://aip.scitation.org/doi/10.1063/1.4915013.
422Supendi, P., Nugraha, A.D., Puspito, N.T., Widiyantoro, S., Daryono, D., 2018.
423 Identification of active faults in West Java, Indonesia, based on earthquake
424 hypocenter determination, relocation, and focal mechanism analysis.
425 Geosci. Lett. 5, 31. https://doi.org/10.1186/s40562-018-0130-y.
426Surono, Jousset, P., Pallister, J., Boichu, M., Buongiorno, M.F., Budisantoso, A.,
427 Costa, F., Andreastuti, S., Prata, F., Schneider, D., Clarisse, L., Humaida,
428 H., Sumarti, S., Bignami, C., Griswold, J., Carn, S., Oppenheimer, C.,
429 Lavigne, F., 2012. The 2010 explosive eruption of Java's Merapi volcano

—A “100-year” event. J. Volcanol. Geotherm. Res. 241–242, 121–135. https://doi.org/10.1016/j.jvolgeores.2012.06.018

Utama, M.R.J., Nugraha, A.D., Puspito, N.T., others, 2015. Seismicity studies at Moluccas area based on the result of hypocenter relocation using hypoDD. AIP Conf. Proc. 1658, 030022. https://doi.org/10.1063/1.4915030.

van Hinloopen Labberton, D., 1921. Oud-Javaansche gegevens omtrent de vulkanologie van Java. Djdwd 1:185-201.

Wagner, D., Koulakov, I., Rabbel, W., Lühr, B.-G., Wittwer, A., Kopp, H., Bohm, M., Asch, G., MERAMEX Scientists, 2007. Joint inversion of active and passive seismic data in Central Java. Geophys. J. Int. 170, 923–932. https://doi.org/10.1111/j.1365-246X.2007.03435.x.

Waldhauser, F., 2001. hypoDD-A Program to Compute Double-Difference Hypocenter Locations (USGS Numbered Series No. 2001–113), Open-File Report. https://doi.org/10.3133/ofr01113.

Waldhauser, F., Ellsworth, W.L., 2000. A double-difference earthquake location algorithm: Method and application to the northern Hayward fault, California. Bull. Seismol. Soc. Am. 90, 1353–1368. https://doi.org/10.1785/0120000006.

Wessel, P., Smith, W.H.F., 1998. New, improved version of Generic Mapping Tools Released. EOS Trans., AGU 79, 579, doi: 10.1029/98EO00426.

Widiyantoro, S., Pesicek, J., Thurber, C., 2011. Subducting slab structure below the eastern Sunda arc inferred from non-linear seismic tomographic imaging. Geol. Soc. London Spec. Pub. 355, 139–155. https://doi.org/10.1144/SP355.7.

Widiyantoro, S., Ramdhan, M., Métaxian, J.-P., Cummins, P.R., Martel, C., Erdmann, S., Nugraha, A.D., Budi-Santoso, A., Laurin, A., Fahmi, A.A., 2018. Seismic imaging and petrology explain highly explosive eruptions of Merapi Volcano, Indonesia. Sci. Rep. 8, 13656. https://doi.org/10.1038/s41598-018-31293-w.

Widiyantoro, S., van der Hilst, R., 1996. Structure and evolution of lithospheric slab beneath the Sunda arc, Indonesia. Science 271, 1566. doi: 10.1126/science.271.5255.1566.

Table 1

Reference 1-D P- and S-wave velocity models. The Vp model is taken from Koulakov et al. (2007).

Depth (km)	Vp (km/s)	Vs (km/s)
-3	4.30	2.49
3	4.90	2.83
8	5.70	3.29
16	6.90	3.99
24	7.10	4.10
77	7.80	4.51
120	8.05	4.65
165	8.17	4.72

210	8.30	4.80

Table 2

Three-dimensional grid spacing used in the tomographic inversions. The center of the model is at 110.45°E and 7.54°S.

Grid direction	Grid distances from the center of the model (km)
x	-500 -350 -160 -120 -80 -50 -30 -20 -10 0 10 20 30 50 80 120 200 500
y	-600 -450 -80 -50 -30 -20 -10 0 10 20 30 50 80 250 400
z	-200 0 5 10 15 20 25 30 35 50 80 110 150 200 590 700

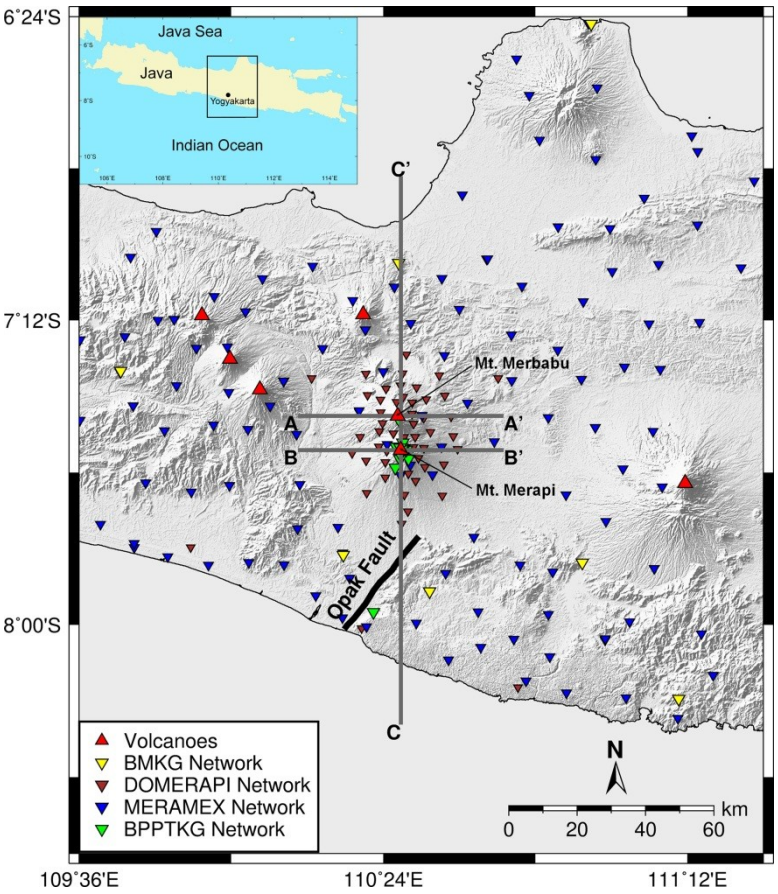

488

489**Fig. 1.** Map of the study region and the distribution of seismographic stations of
490the DOMERAPI, MERAMEX, BPPTKG and BMKG networks. Red triangles to
491the north of the Opak fault depict the locations of the Merapi and Merbabu
492volcanoes. See the legend in the inset for the definition of symbols used on the
493map. Lines A-A' and B-B' depict the locations of vertical sections shown in Figs.
4944 – 7, and Line C-C' depicts the location of deep vertical sections shown in Figs.
495S7 and S8.

496

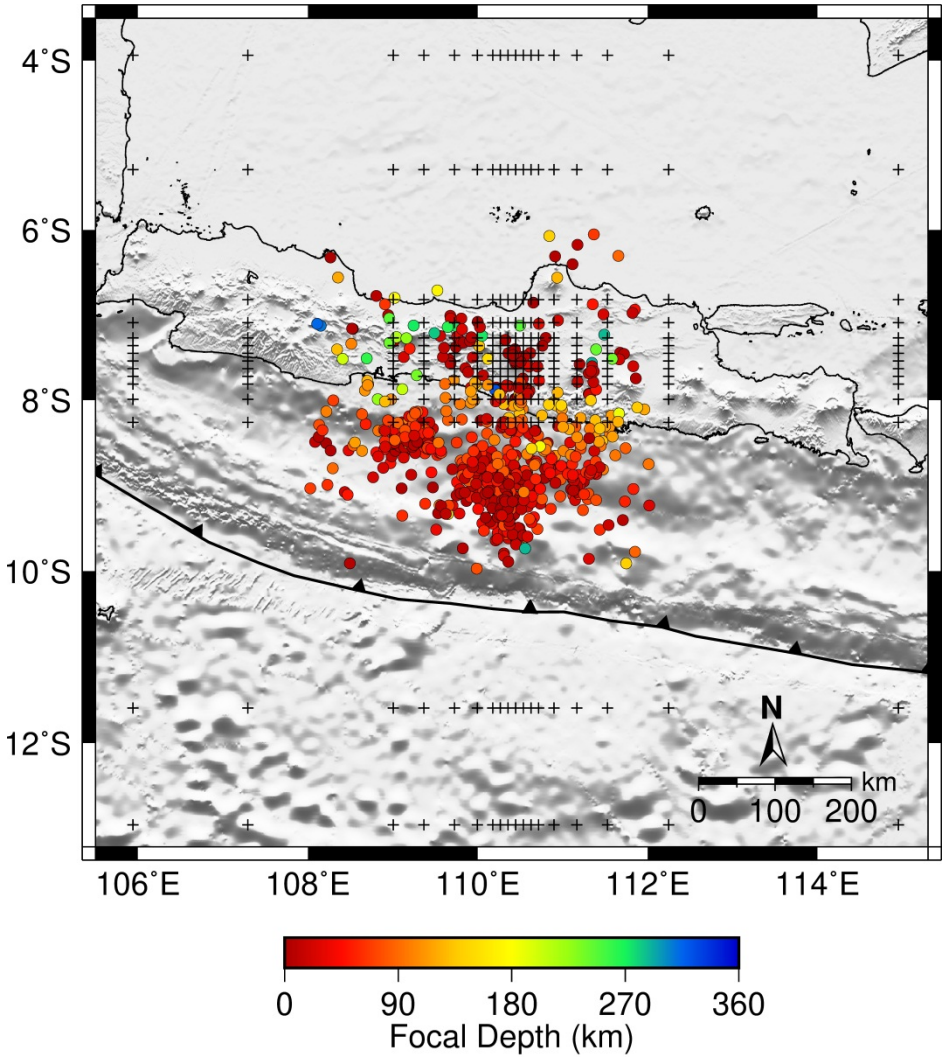

497

498**Fig. 2.** Configuration of grids used for seismic tomographic imaging and the

499distribution of epicenters produced by SIMULPS12.

500

501

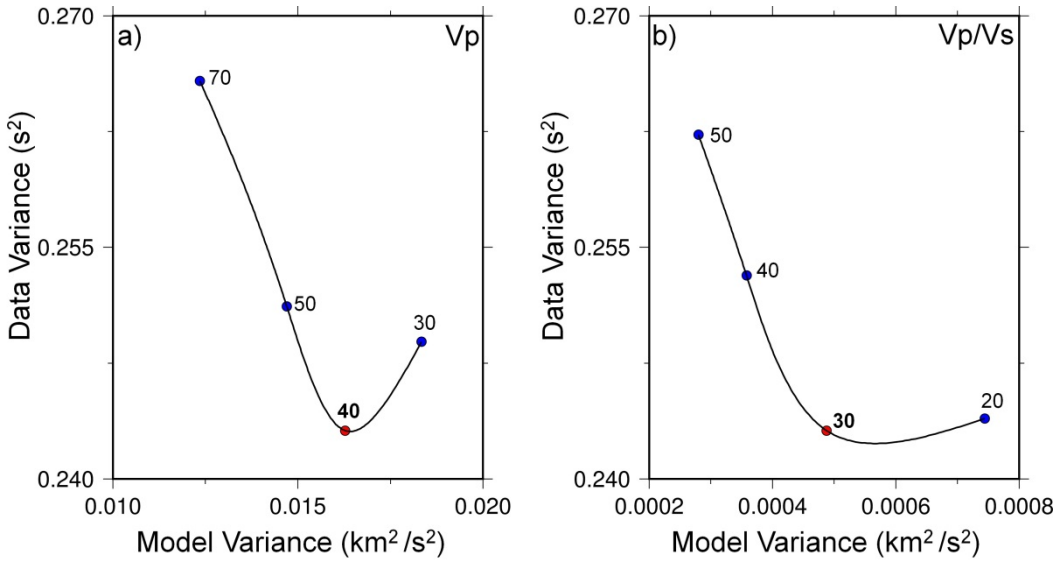

Fig. 3. Trade-off curves showing model variance versus data variance, which is used for selecting optimal damping values. a) Damping values of 40 for Vp, and b) 30 for Vp/Vs (red dots), with a station damping value of 10, are selected for the inversions. The model and data variance are computed after one iteration for the indicated damping values. Note that when the damping values are too small (rightmost points), the velocity tends to oscillate from one grid point to the next, and strong velocity anomalies are introduced without significant reductions in data variance (Eberhart-Phillips, 1986; see also Widiyantoro et al., 2018).

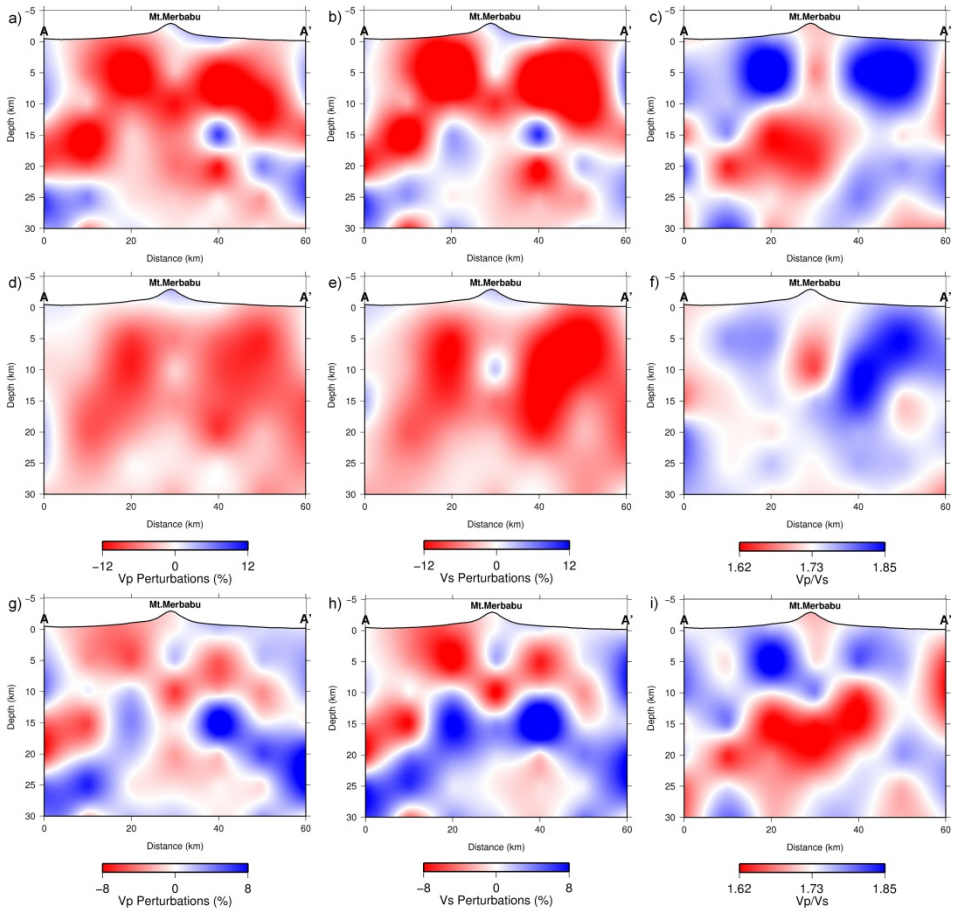

512

513**Fig. 4.** West-east (A-A') vertical sections across Mt. Merbabu through a) Vp, b)
514Vs, and c) Vp/Vs models from joint inversions using the full data set (from
515DOMERAPI, MERAMEX, BMKG, and BPPTKG); d-f) similar to a-c, but
516without the DOMERAPI data; and g-i) the difference between a-c and d-f plotted
517with a more restricted perturbation scale (±8%) to illustrate the improvement due
518to the inclusion of DOMERAPI data. Note that depth = 0 km depicts MSL.

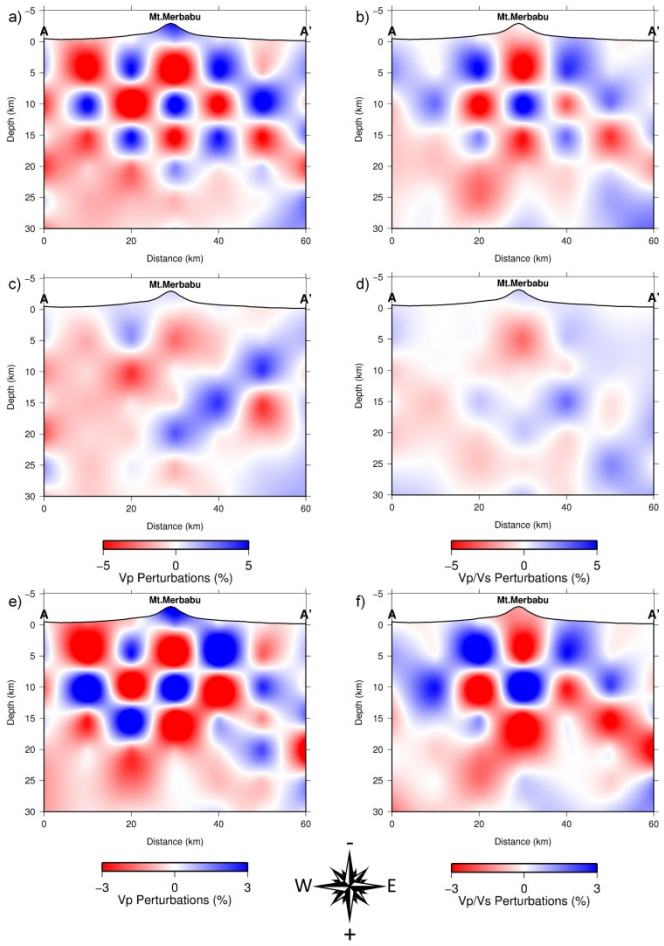

519

520**Fig. 5.** Results of the checkerboard test for vertical sections A-A'. a) Vp and b)
521Vp/Vs from joint inversions using the full data set; c-d) similar to a-b, but without
522the DOMERAPI data; e-f) the difference between a and c, and b and d,
523respectively. Note that the checkerboard recovery of Vs is similar to the one for
524Vp/Vs.

525

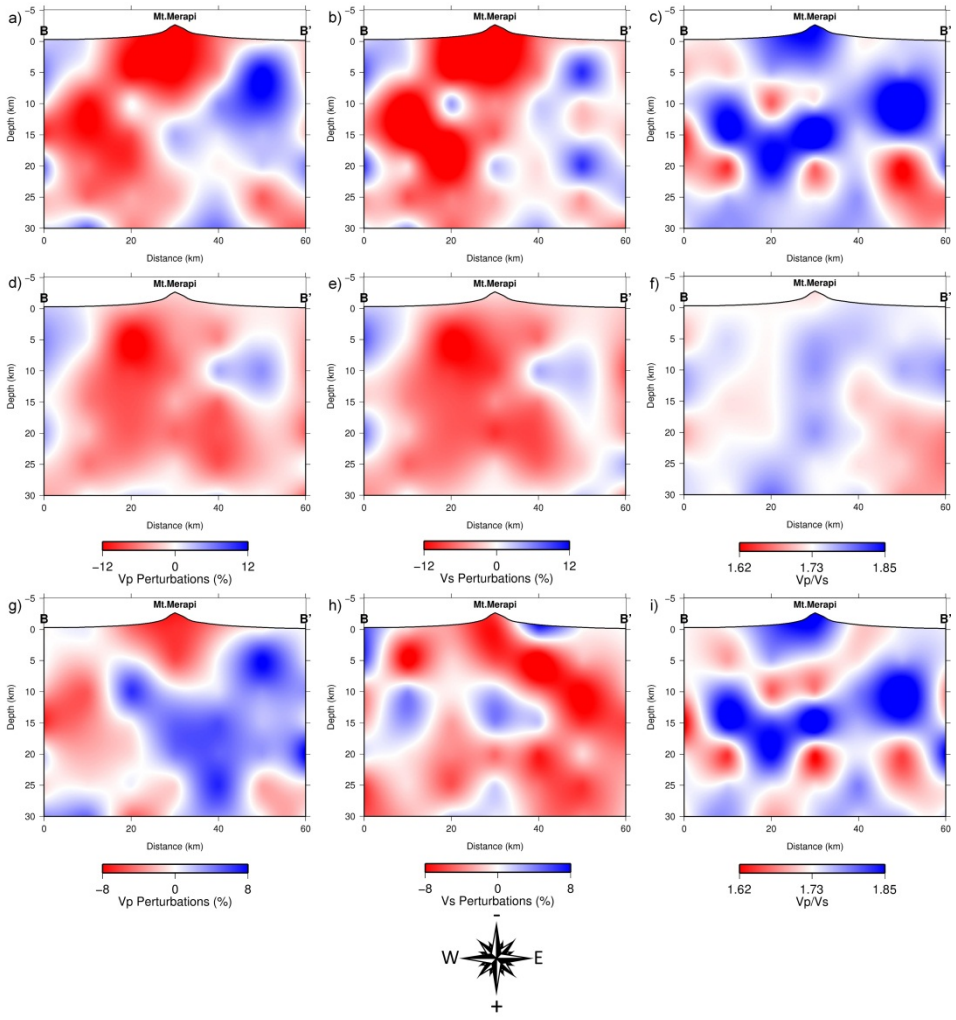

526

527**Fig. 6.** Same as Fig. 4, except for west-east (B-B') vertical sections across Mt.

528Merapi.

529

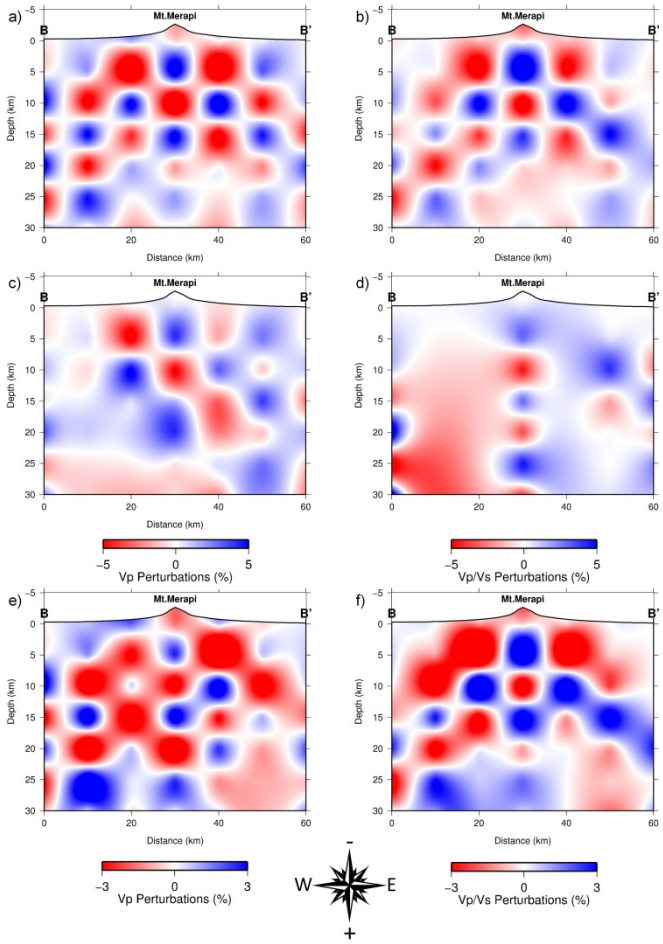

530

531**Fig. 7.** Same as Fig. 5, except for B-B' vertical sections across Mt. Merapi.

532

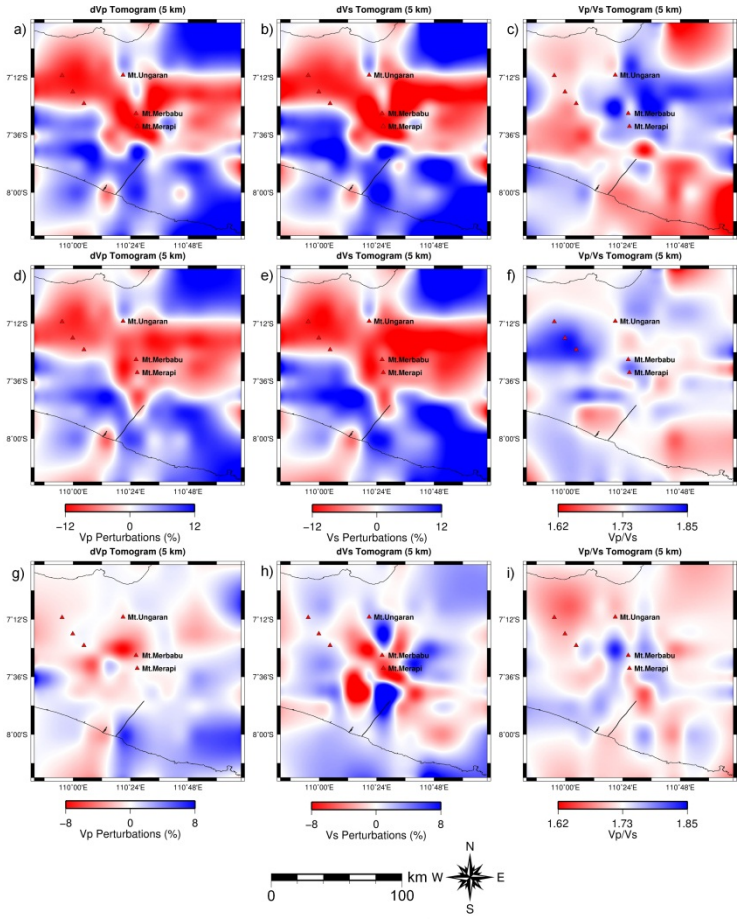

533

534**Fig. 8**. Horizontal slices at 5 km depth below MSL through a) Vp, b) Vs, and c)
535Vp/Vs models from joint inversions using the full data set; d-f) similar to a-c, but
536without the DOMERAPI data; g-i) the difference between a-c and d-f plotted with
537a more restricted perturbation scale (±8%) to demonstrate the improvement due to
538the inclusion of DOMERAPI data.

539

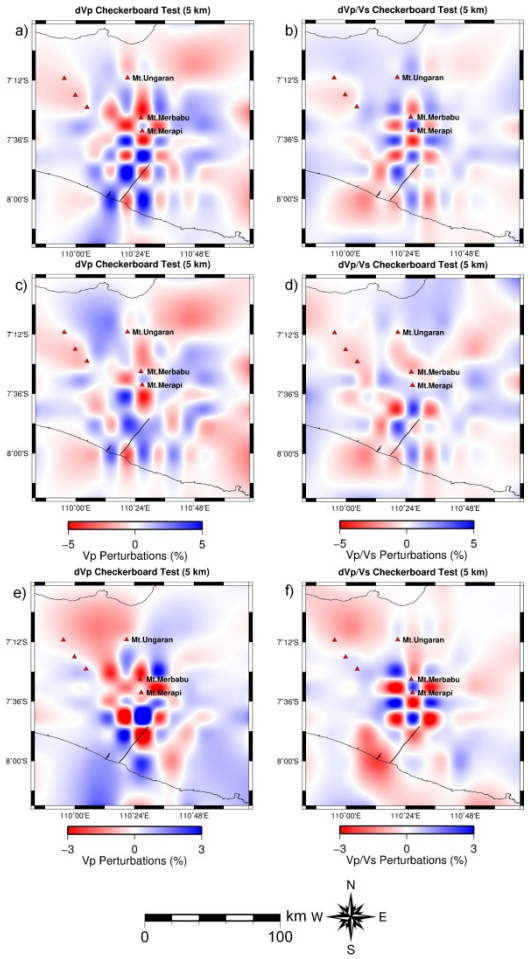

Fig. 9. Results of the checkerboard test for horizontal slices at 5 km depth. a) Vp and b) Vp/Vs from joint inversions using the full data set; c-d) similar to a-b, but without the DOMERAPI data; e-f) the difference between a and c, and b and d, respectively. Note that the checkerboard recovery of Vs is similar to the one for Vp/Vs.